Absorbable Mineral Nanocomposite for Biomedical Applications: Influence of Homogenous Fiber Dispersity on Mechanical Properties

Elias Mulky [a, b], Katharina Maniura-Weber [b], Martin Frenz [d], Giuseppino Fortunato *[c], Reto Luginbuehl[e]

a RMS Foundation, Bischmattstrasse 12, Bettlach, Switzerland

b Empa, Swiss Federal Laboratories for Materials Science and Technology, Laboratory for Biointerfaces, Lerchenfeldstrasse 5, 9014 St Gallen Switzerland

c Empa, Swiss Federal Laboratories for Materials Science and Technology, Laboratory for Biomimetic Membranes and Textiles, Lerchenfeldstrasse 5, 9014 St Gallen, Switzerland

d University of Bern, Institute of Applied Physics, Sidlerstrasse 5, 3012 Bern, Switzerland

e University of Bern, Department of Biomedical Material Research, 3002 Bern, Switzerland

*E-mail address: pino.fortunato@empa.ch

KEYWORDS: absorbable, Calcium Phosphate Cement, Composite, Nanofibers, electrospinning

This document is the accepted manuscript version of the following article:
Mulky, E., Maniura-Weber, K., Frenz, M., Fortunato, G., & Luginbuehl, R. (2017). Absorbable mineral nanocomposite for biomedical applications: influence of homogenous fiber dispersity on mechanical properties. Journal of Biomedical Materials Research. Part A. http://doi.org/10.1002/jbm.a.36284

Abstract: Electrospun micro- and nano-sized fibers are frequently used as reinforcing elements in low temperature ceramic composites for biomedical applications. Electrospinning of fibers yield, however, not individual fibers, but rather fiber-mats that are difficult to separate. Most investigations have been performed on diced mats and highly non-homogenous composites. We examined the influence of dispersed electrospun single micro- and nano-meter fibers on the mechanical properties of calcium phosphate cement composites. Absorbable Poly-L-Lactic-Acid (PLLA) was electrospun yielding fibers with diameters of 244 ± 78 nm, named nanofibers (NF), and 1.0 ± 0.3 μm, named microfibers (MF). These fibers were cut using a particle assisted ultrasonication process and dispersed with Hydroxyapatite (HA) nanoparticles and composites of low (5%) and high (30%) NF/MF content were engineered. The homogeneity of the fiber distribution was investigated by analyzing fracture areas regarding the number of fibers and Voronoi area size distribution. Variation of fiber distribution was significantly lower in the NF group as compared to the MF group. For composites containing 5% NF (V/V), an 8-fold increase in the compressive fracture strength, and for the 30% NF (V/V) a 3-fold increase compared was measured. The composite containing 5 % NF was identified as optimal regarding fiber distribution and strength. Our new method of engineering these composites allows for high volume fractions of NF with low variation in fiber distribution to be incorporated into composites, and shows the importance of using single filaments as reinforcing agents.

1. INTRODUCTION

Calcium phosphate cements (CaP) are frequently used as defect fillers for human bones [1]. They are well-accepted by the bone tissue and are absorbed within specified time frame based on their formulation [2]. The drawback of CaP are, however, their poor mechanical properties [3], which limits their use to non-load bearing situations. That drawback can be overcome by introducing reinforcing elements in form of fibers [4-6]. The resulting mechanical properties of such so-called fiber reinforced composites (FRC) outperform typically those of the matrix or fibers alone. In particular, in cements, the aggregation of crystalline nano- and micro particles forms a brittle, porous bulk structure. Under load, these cements tend to fracture without a prior discernible change in geometry or mechanical properties, resulting in a sudden significant loss of mechanical properties.

Nowadays, fibers are widely used as additives in cements. Von Gonten and colleagues used a polyglycolic acid based multifilament fiber meshes with single filament diameters of 17 μm to reinforce a hydroxyapatite (HA) based matrix resulting in a composite with the work of fracture (29 N/m) equal to that of PMMA (28 N/m) in flexural strength [7]. In a similar approach, Xu and co-workers used a variety of different discontinuous filaments of Aramid, E-glass or polyglycolic acid with diameters in the order of tens of micrometers and lengths between 3 and 200 mm to reinforce HA. They described an up to four-fold increase in fracture strength as compared to their pristine cement control [6]. However, at fiber contents above 5%, the fibers entangled which lead to phase segregation within the cement and consequently to a lower reinforcement and even a decrease in strength. This is a prime example for the importance of homogeneous fiber dispersion for yielding matrix reinforcement. In that context, it can be conjectured that decreasing the fiber diameters while keeping the total fibrous volume constant allows for a significantly larger part of the cement matrix to be in

contact with the fibers. The consequence is an increased reinforcement provided that the fiber aspect ratio is constant or larger than in the case of larger diameter fibers [4, 8, 9].

Electrospinning is a well-established technique to engineer micro- and nanometer-sized fibers from a large selection of polymeric and inorganic materials [10-13]. The process typically yields directionally or randomly oriented fibers which are collected in the form of non-woven fleece [10, 14, 15]. Such mats are however not suited for reinforcement as they cannot be homogenously dispersed in or penetrated by the matrix material such as calcium phosphate based cements. It has been shown that their effect in composites is minimal or non-existing even they were chopped into multi filament segments prior to use [16]. The direct engineering of short, staple fiber like fibers by electrospinning has been demonstrated [17]. It either results in rather slow process (solution flow rate of 0.5 µL/min), or is restricted to polymers with rather low molar mass in the range of 15 kDa [18]. In order to produce strong composites, polymers with high molar mass are desirable in the production of mechanical competent composites [19]. In order to obtain staple fibers from electrospinning process at high yield, post-processing is required to separate and cut these meshes into single separated filaments. We recently demonstrated that electrospun PLLA fibers can be separated and cut to staple fiber like precursors by using a particle assisted sonication process [20].

It is the aim of the present work to show the effect of fiber dispersion in calcium phosphate based cements on the fracture strength. Our approach lies in engineering composites containing hydroxyapatite nanoparticles as base and use them for particle assisted sonication allowing for high intercalation and penetration of the fibrous phase yielding a homogenous distribution. The resulting particle/fiber mixture is reacted with monocalcium phosphate monohydrate and water to obtain a rapidly degradable monetite/brushite cement [21, 22]. Electrospun PLLA fibers with diameters of 250 nm (NF) or 1000 nm (MF) were used as fibers. These diameters were chosen to study the influence of fiber dispersity within the same

volume fraction at low (5%) and high (30%) concentrations. Cements containing diced electrospun mats served as negative control. Furthermore, the influence of the fiber content on the phase composition of the CaP based cement was evaluated by comparing the composites with pristine cement of similar water content. The resulting composites were comprehensively characterized regarding compressive strength, crystalline phase composition as well as fiber dispersity.

2. MATERIALS AND METHODS

All solvents were obtained from commercial providers in ACS quality and were used without further purification. Poly-L-Lactic Acid (PLLA, Biomer L9000, Mm: 200 000 Da) was obtained from Biomer Biopolyesters (Krailing, Germany). Chloroform, N-N-dimethylformamide, formic acid, and disodium dihydrogen pyrophosphate, were purchased from Sigma Aldrich (Buchs, Switzerland). Hydroxyapatite (HA) nanoparticles were purchased from MKnano (Missisauga, ON, Canada) and monocalcium phosphate monohydrate particles (MCPM, Regent 12xx) were purchased from Innophos Inc. (Cranbury NJ, USA).

2.1. FIBER PROCESSING

The polymer fibers were manufactured by electrospinning. The protocol for electrospinning was described in previous work [20] and adapted for the present study: Briefly, 5.6% (w/w) of PLLA for nanofiber (NF) production and 8.9% (w/w) PLLA for microfiber (MF) production were dissolved in a solution containing chloroform : DMF at a ratio of 8:1 (w/w). The solutions were mixed for at least 15 h at room temperature on an orbital shaker (200 rpm) prior to use. After complete dissolution of the PLLA, an aliquot of stock solution was separated for immediate use for electrospinning and concentrated formic acid was added slowly while mixing to achieve a ratio of 9:1 (w/w) of stock solution to formic acid. The resulting solution was incubated again for 20 min on the orbital shaker.

Electrospinning was performed with an in-house built device, consisting of a syringe pump Aladdin 1000 (World Precision Instruments, Sarasota, FL, USA), a variable high voltage power source CPS Series (AIP Wild AG, Oberglatt, Switzerland), and an in-house built rotating collector which allowed for predominate fiber orientation. The complete system was placed in a Faraday cage. A +15/-5 kV potential, with a maximum current of 0.1 mA, was applied between the 18G, blunt needle tip (BD

Braun, Bethlehem, PA, USA) and collector with a tip-collector distance of 18 cm. The rotating speed of the 20-cm diameter collector was constant at 1340 rpm. An in-house programmed LabVIEW ™ application was used to control the electrospinning process. Collected fibers were removed from the collector using a surgical blade and a metal tweezers and wrapped in aluminum foil for storage before post processing.

2.2. FIBER ANALYSIS

The fibers were analyzed using scanning electron microscopy (SEM). The samples were coated with 7 nm of gold using a sputter coater Polaron. E5100 (Polaron Equipment Ltd., Hertfordshire, United Kingdom). SEM analysis was conducted on a Hitachi S-4800 (Hitachi Ltd., Tokyo, Japan) using a voltage of 2 kV and 10 μA of current. The diameters of at least 10 fibers from three separate images were measured per batch.

2.3. COMPOSITE PROCESSING

The protocol for composite engineering was described in detail in a previous work and adopted accordingly [20]. Briefly, the collected fiber meshes were removed from the aluminum wrapping with tweezers and diced to approximately 1 cm x 1 cm sections using a surgical blade no 11, sterile (KLS Martin Group, Mühlheim, Germany), preferentially perpendicular to the main fiber orientation. Subsequently, the patches were transferred into a 30 mL glass flask containing 20 mL of n-hexane. The flask was then immersed in a dry ice/acetone bath and cooled to -80 °C. The bath temperature was maintained constant during the process by periodically refilling the coolant mixture. HA nanoparticles with a nominal diameter of 30 nm were added at a ratio of 5:1 w/w for the cement precursor containing 5% v/v of fibers and 9:10 w/w for the cement precursor containing 30% v/v of fibers, respectively.

Sonication was performed by immersing a 1.27 cm sonicator tip (Branson Digital Sonifier Model 450D, 20 kHz fixed frequency, 400 W output power, Emerson, Ferguson, MO, USA) for 30 min in 2/2 s on/off cycles at an amplitude of 90%. Multiple batches of 50 to 80 mg PLLA fibers were sonicated summing up samples of up to 1000 mg (fibers and HA particles). In a final step, MCPM was added at a ratio of 16:13 HA-fiber premix to MCPM and sonicated again for 5 min. The resulting fiber/particle dispersion was drained of excess hexane using a filter, and air dried in a fume hood under ambient conditions for at least 15 h.

An aqueous solution containing 0.06 M disodium dihydrogen pyrophosphate, which slows the setting reaction and maintain moldability during handling [23]. was prepared with deionized water (>18 MΩ, in-house supply). This liquid was mixed with the HA/PLLA/MCPM at ratios of 9:4, 8:4 and 7:4 dry powder mixture to liquid ratio (w/w). The ratios were calculated for the composite to have a fiber content of 0%, 5% and 30% v/v respectively. Additional pristine (containing no fibers) cements with powder to liquid ratios of 8:4 and 7:4 were produced as controls, corresponding to the added liquid of the composites containing fibers at 5% and 30% v/v. The resulting slurry was mixed for 2 min with a spatula to obtain a cement paste, which was transferred into custom-made Teflon cylinders of 5 mm diameter and 7 mm height. The cement allowed for setting and curing during 3 days in a fume hood under dry conditions.

Non-sonicated controls were produced by dicing PLLA fiber meshes to 10 mm x 10 mm sections, and mixing them with HA and MCPM at the ratios as indicated above. The cement paste was mixed manually using a spatula and vortexed for 15 s.

2.4. COMPOSITIONAL ANALYSIS OF THE CEMENTS

The different crystalline calcium phosphate phases were analyzed using X-ray diffraction analysis (XRD). The samples were prepared by manual milling in an agate mortar (Agar Scientific Ltd, Stansted, United Kingdom). The resulting powders were spread in a cylindrical poly-methyl-methacrylate (PMMA) sample holder. Samples containing less than 1 g total mass were processed by adding acetone to the powder mass to form a slurry and spread directly in the sample holders. All XRD measurements were either performed on a X'Pert Pro MPD (Panalytical, Almelo, The Netherlands) or on a Bruker D8 ADVANCE (Bruker Corporation, Billerica MA, USA) diffractometer. Ni-filtered CuK_2 x-ray source was used and spectra were acquired between 4.01° and 59.99° with a step size of 0.016°. For the non-sonicated controls, the device used was a. The peaks were semi quantitatively analyzed by Rietveld refinement using BGMN software (http://profex.doebelin.org). Crystalline models of the BGMN database were used.

2.5. MECHANICAL CHARACTERIZATION OF THE CEMENTS

Static compressive strength was determined on a Zwick 1474 universal testing machine (Zwick GmbH, Ulm, Germany) using cylindrical samples of 5 mm diameter and 7 mm height. Fracture was determined to be at the point of maximum compressive force.

2.6. FRACTURE PLANE ANALYSIS

All fracture planes of the samples were coated with gold using a sputter coater SCD 050 (Baltec, Pfäffikon, Switzerland) prior to scanning electron microscopy analysis using a Zeiss MA 26, (Zeiss AG, Oberkochen, Germany). The fiber distribution in the composite materials was analyzed by acquiring 10 micrographsat 2000-fold magnification in random areas on one sample of each group. The micrographs were analyzed using the Fiji distribution of the imageJ software, Version 1.50i (National Institute of Health, Bethesda, USA). The fibers were marked at the exit points from the cement and counted manually on each image using the cell-counting package of imageJ. In addition, the protocol for Voronoi/Delaunay analysis was adapted from Bertoncelj and co-workers for use on a rough surface [24]. Briefly, the Voronoi surface around each fiber is the area that is closer to that fiber than to any other fiber. It was iteratively measured using the imageJ plugin. The values used for analysis were the following. (a) Average number of fibers over all images $\bar{x}(f)$ was used as measure to differentiate between the dispersity between nano- and microfibers. (b) Standard deviation of number of fibers $\sigma(f)$ was used to measure the variation between the number of fibers within the images. (c) Coefficient of variation of fibers $\gamma(f)$ is the standard deviation of the fiber number divided by average number of fibers. (d) Voronoi surface area ν is the area containing all points closer to one fiber than to any another. (e) Area homogeneity coefficient $\gamma(v)$ is the average coefficient of variation for the Voronoi surface areas. (f) Standard deviation of the area homogeneity coefficient $\sigma(\gamma(v))$, which indicates how homogeneous the composite is overall between the images.

106 **2.7. STATISTICAL ANALYSIS**

The statistical analysis was conducted using one- or two-way ANOVA where appropriate. Sample sizes
108 and repetitions are indicated in the methods section of the respective experiment. The analysis was performed using Origin 8.1 software. P values < 0.05 considered as significant.

3. RESULTS AND DISCUSSION

3.1. FIBER MANUFACTURING

The acid-containing polymer solutions were spun for 5 h on a high-speed rotating collector. The NF exhibited a smooth surface morphology. Very little bead formation was observed in the mesh (figure 1 a, b). The MF (figure 1 c, d) on the other hand, exhibited a slightly rougher surface. This wrinkling along the fiber axis is due to the interaction of the fiber jet with humidity from the environment [25] which in the current case was observed to be between 45 and 60%. The average diameter of the obtained PLLA fibers was determined based on SEM micrographs and was found to be 0.24 ± 0.08 μm for the NF and 1.0 ± 0.2 μm for the MF. These fibers were post processed to be used in the composites.

3.2. COMPOSITE PROCESSING

The powder phases containing the cement and the fiber phase were mixed with the liquid phase to create a cement. It was observed that when being poured into 1.5 mm diameter forms, the moldability was in the following order: pristine cement > 5% sonicated > 30 % sonicated >5% non-sonicated > 30% non-sonicated whereas NF or MF containing fraction did not matter. It was noted that the liquid to powder ratio had to be increased for complete wetting from the initial 4:9 (w/w) for pristine cements to 4:8 (w/w) for 5% fiber and 4:7 (w/w) for 30% fiber content. This change in moldability is due to fiber agglomeration during the mixing process of samples with high fiber contents and is in agreement with the observation by Martinie and co-workers [26]. Agglomeration was also observed by Xu and co-workers during hydroxyapatite reinforcement with a fiber volume fraction of 9.5% v/v [6]. Regardless of fiber distribution, it is necessary to take the fiber content into account when adding the aqueous phase.

3.3. COMPOSITION ANALYSIS OF THE CEMENTS

The reactivity, defined as residual amounts of HA and MCPM, of the cement decreased with increased fiber content as measured with XRD. An example of the refinement is shown in the supplementary data in figure S1. There is trend that the fraction of unreacted HA and MCPM increased with fiber content and sonication (Figure 2). No significant difference in the reactivity in between the MF group was observed. Furthermore, it was observed that a notable amount of MCPM was present in the samples containing 30% of NF, and in samples with increased water content. Thus, it can be hypothesized that reactivity of the MCPM is reduced in the surrounding of the fibers. Due to the significantly larger surface area of the NF composites (a calculated 16x surface increase compared to the micro phase) the effect is more pronounced in composites containing NF.

XRD analysis of the products dicalcium phosphate dihydrate (brushite) and dicalcium phosphate anhydrous (monetite) revealed a lower content of brushite in the cements containing sonicated fibers when compared to pristine cements. The non-sonicated composites however contained increasing contents of brushite with increased fiber content. Again, it can be hypothesized that the presence of fibers inhibits the uptake of water by influencing the cement reaction towards monetite formation. The increased content of both monetite and brushite correlated with an increase in strength, while an increase in hydroxyapatite content led to a decrease in strength in the fiber reinforced composites.

3.4. MECHANICAL CHARACTERIZATION OF THE COMPOSITES

All composites were tougher than the corresponding pristine cements. While pure hydroxyapatite has been observed to have a significantly higher compressive strength of up to 70 MPa compared to brushite or monetite, (up to 10 MPa) [3], the mixture of both phases resulted in a significantly lower compressive

strength of <2 MPa for the pristine cements. The increase in composite strength can therefore be attributed to the presence of the reacted components rather than to the amount of hydroxyapatite present. Analysis of the mechanical properties resulted in an increase in compressive strength of the FRC as compared to the pristine cement or the non-sonicated counterparts (Figure 3). The results of the sonicated composites were significant regarding to both fiber content and fiber diameter. Especially notable was the 5% v/v NF cement achieved the highest (eight-fold) reinforcement of all groups as compared to the pristine cement. This is in accordance with the results reported by Xu and co-workers [5], who observed a peak in flexural strength at approximately 7.5% polyglactin fiber content in a hydroxyapatite composite. Our results show that already 5% of fibers (v/v) is sufficient to achieve a measurable increase in compressive strength in the cement (for both NF and MF). Increasing the fiber content to 30% did not yield an increased strength of the composite as compared to the 5% content, and in the case of the non-sonicated controls and MF, plastic deformation was observed. We assume that the fragments of the mats present within these composites greatly influenced the compressive modulus of the composite. Therefore, the influence of the fiber phase on the compressive modulus is dominant at 30% volume content.

3.5. FRACTURE ANALYSIS

Analysis of the fracture areas (Figure 4 a-h) showed a significant amount of unclad fibers dangling from the fracture area. It can therefore be concluded that the primary mechanism of composite fracture is mainly by fiber pull-out, which is to be expected since PLLA fibers are more hydrophobic (water contact angle of 70° [27]) as compared to the more hydrophilic CaP matrix. Analysis of the fiber distribution on the fracture area (Figure 5, Table 1) showed that the average number of non-aggregated

fibers per image was significantly higher in the 5% and 30% NF composites (180±60, 190±54) as compared to the number of fibers on the fracture areas of 5% and 30% MF composites, (25±28, 55±30). The variation in number of fibers between the images of the same group divided by the average fiber number (coefficient of variation) was significantly lower in the NF composites (0.3, 0.3), as compared to the microfiber composites (1.1, 0.6). The results were significant regarding fiber diameter but not regarding the fiber content. Additional analysis showed that no significant differences were observed between the 5% and 30% NF groups while the difference between the 5% and 30% MF was significant. Due to the manual processing of the composites, it is possible that they were not completely homogeneous. It can be assumed that the fracture areas analyzed were areas with lowest reinforcement, containing the lowest number of fibers. Furthermore, due to the low number of samples analyzed for their fracture areas, it is possible that the 30NF sample contained a low amount of fibers at the fracture site. The Voronoi areas were similar in the NF group (16 ± 6, 14 ± 5), and significantly different within the MF group (440 ± 740, 66 ± 36). It can be assumed from the lower variation of the 30% NF/MF group compared to the 5% NF/MF that at lower fiber concentrations, the effect of clustered fibers is more pronounced. The non-sonicated cements showed a strong inhomogeneity, i.e. areas with only fibers and areas with only cements, and were therefor excluded from evaluation. It can be thus concluded that a more homogeneous distribution of the fibers can be achieved when using fibers with a smaller diameter, allowing a better intermixing of the components and thus a superior reinforcement. For micro fiber composites, the sonicated materials were comparable to the non-sonicated controls, indicating that while the introduction of fibers increases the compressive strength of the composites, the fiber dispersity of NF is the dominating factor contributing to the compressive strength of the composite.

4. CONCLUSIONS

Absorbable fiber reinforced calcium phosphate based cements were produced via electrospinning, subsequent sonication followed by cement reaction. We found that the highest impact of fiber volume content on the mechanical and structural properties of the fiber reinforced cement was obtained for the 5% v/v fiber fraction. Regardless of fiber content the NF enabled a higher fracture strength as compared to the MF. An inhibition of water uptake to form brushite was observed when fibers were added to the cement mixture. The sonicated NF samples had a higher compressive strength when compared to their non-sonicated counterparts, while the sonicated MF samples had a similar compressive strength when compared to their non-sonicated counterparts. This was independent of crystalline and water content and indicates that indeed the fiber distribution has a large influence on the fracture strength of the composites. Additionally, at high fiber content of 30% (w/w), the composite fracture strength was reduced, but still significantly higher than the pristine cement. The analysis of the fracture area revealed the most homogenous fiber distribution for the 5% sonicated NF. We have thus demonstrated that a good dispersion of NF enhances the fractural strength of calcium phosphate based cements.

5. ACKNOWLEDGEMENTS

This work was supported by a grant of the Swiss National Science Foundation Program "Opportunities and Risks of Nanomaterials" NRP 64, grant no. 406440_131273. The authors would like to thank Stefan Röthlisberger (RMS Foundation) for conducting the mechanical tests, Nicola Döbelin (RMS Foundation) for performing the XRD measurements and Christian May (RMS Foundation) for his help with the Voronoi analysis.

6. REFERENCES

1. Döbelin, N., R. Luginbühl, and M. Bohner, *Synthetic calcium phosphate ceramics for treatment of bone fractures.* Chimia, 2010. **64**(10): p. 723-729.

2. Legeros, R.Z., *Biodegradation and bioresorption of calcium phosphate ceramics.* Clinical Materials, 1993. **14**(1): p. 65-88.
3. Charrière, E., et al., *Mechanical characterization of brushite and hydroxyapatite cements.* Biomaterials, 2001. **22**(21): p. 2937-2945.
4. Beaudoin, J.J., *Handbook of Fiber-Reinforced Concrete*. Building Materials Science Series, ed. I.f.R.i.C. V. S. Ramachandran, National Research Council of Canada. 1990, Ottawa: Noyes Publications. 332.
5. Pirhonen, E., *Fibres and Composites for Potential Biomaterials Applications*, in *Institute of Biomaterials*. 2006, Tampere University of Technology: Tampere. p. 80.
6. Xu, H.H.K., F.C. Eichmiller, and A.A. Giuseppetti, *Reinforcement of a self-setting calcium phosphate cement with different fibers.* Journal of Biomedical Materials Research, 2000. **52**(1): p. 107-114.
7. Von Gonten, A.S., J.R. Kelly, and J.M. Antonucci, *Load-bearing behavior of a simulated craniofacial structure fabricated from a hydroxyapatite cement and bioresorbable fiber-mesh.* Journal of Materials Science: Materials in Medicine, 2000. **11**(2): p. 95-100.
8. Proctor, B.A., *A review of the theory of GRC.* Cement and Concrete Composites, 1990. **12**(1): p. 53-61.
9. Zollo, R.F., *Fiber-reinforced concrete: an overview after 30 years of development.* Cement and Concrete Composites, 1997. **19**(2): p. 107-122.
10. Yan, H., L. Liu, and Z. Zhang, *Continually fabricating staple yarns with aligned electrospun polyacrylonitrile nanofibers.* Materials Letters, 2011. **65**(15–16): p. 2419-2421.
11. Peng, J., et al., *Preparation and release characteristic of quercetin loaded poly(lactic acid) ultrafine fibers.* Journal of nanoscience and nanotechnology, 2011. **11**(4): p. 3659-3668.
12. Yao, L., C. Lee, and J. Kim, *Fabrication of electrospun meta-aramid nanofibers in different solvent systems.* Fibers and Polymers, 2010. **11**(7): p. 1032-1040.
13. Greiner, A. and J.H. Wendorff, *Electrospinning: A fascinating method for the preparation of ultrathin fibers.* Angewandte Chemie - International Edition, 2007. **46**(30): p. 5670-5703.
14. Simonet, M., et al., *Ultraporous 3D polymer meshes by low-temperature electrospinning: Use of ice crystals as a removable void template.* Polymer Engineering and Science, 2007. **47**(12): p. 2020-2026.
15. Yang, J.C., et al., *Formation of highly aligned, single-layered, hollow fibrous assemblies and the fabrication of large pieces of PLLA membranes.* Macromolecular Materials and Engineering, 2012. **297**(2): p. 115-122.
16. Zuo, Y., et al., *Incorporation of biodegradable electrospun fibers into calcium phosphate cement for bone regeneration.* Acta Biomaterialia, 2010. **6**(4): p. 1238-1247.
17. Fathona, I.W. and A. Yabuki, *One-step fabrication of short electrospun fibers using an electric spark.* Journal of Materials Processing Technology, 2013. **213**(11): p. 1894-1899.
18. Greenfeld, I. and E. Zussman, *Polymer entanglement loss in extensional flow: Evidence from electrospun short nanofibers.* Journal of Polymer Science, Part B: Polymer Physics, 2013. **51**(18): p. 1377-1391.
19. Nunes, R.W., J.R. Martin, and J.F. Johnson, *Influence of molecular weight and molecular weight distribution on mechanical properties of polymers.* Polymer Engineering & Science, 1982. **22**(4): p. 205-228.
20. Mulky, E., et al., *Fabrication of biopolymer-based staple electrospun fibres for nanocomposite applications by particle-assisted low temperature ultrasonication.* Materials Science and Engineering: C, 2014. **45**: p. 277-286.
21. Theiss, F., et al., *Biocompatibility and resorption of a brushite calcium phosphate cement.* Biomaterials, 2005. **26**(21): p. 4383-4394.

22. Desai, T.R., S.B. Bhaduri, and A.C. Tas. *A self-setting, monetite (CaHPO4) cement for skeletal repair*. in *Advances in Bioceramics and Biocomposites II - 30th International Conference on Advanced Ceramics and Composites*. 2006. Cocoa Beach, FL.
23. Bohner, M., J. Lemaitre, and T.A. Ring, *Effects of sulfate, pyrophosphate, and citrate ions on the physicochemical properties of cements made of β-tricalcium phosphate-phosphoric acid-water mixtures.* Journal of the American Ceramic Society, 1996. **79**(6): p. 1427-1434.
24. Bertoncelj, B., et al., *A Voronoi-diagram analysis of the microstructures in bulk-molding compounds and its correlation with the mechanical properties.* Express Polymer Letters, 2016. **10**(6): p. 493-505.
25. Yazgan, G., et al., *Steering surface topographies of electrospun fibers: understanding the mechanisms.* Scientific Reports, 2017. **7**(1): p. 158.
26. Martinie, L., P. Rossi, and N. Roussel, *Rheology of fiber reinforced cementitious materials: classification and prediction.* Cement and Concrete Research, 2010. **40**(2): p. 226-234.
27. Thanki, P.N., E. Dellacherie, and J.-L. Six, *Surface characteristics of PLA and PLGA films.* Applied Surface Science, 2006. **253**(5): p. 2758-2764.

294 **Legend to Table and Figures**

Table 1: Average number of fibers as determined manually from the SEM micrographs. Voronoi
296 surface areas as measured by software and calculated values as derived from section 2.6.

298 Figure 1: SEM micrographs of pristine PLA NF (a, b) and MF (c, d) as spun on a rotating collector imaged at low (a, c) and high (b, d) magnification. Visible is the smooth structure of the NF
300 b), and the wrinkled structure of the MF d).

302 Figure 2: XRD analysis of the relative (% mass) crystalline content of the sonicated composites. Brushite and monetite are the products, while MCPM and Hydroxyapatite are the starting
304 materials. There is a trend of decrease in reactivity with increased fiber dispersion and fiber content. The numbers in the bars refer to respective mass fraction.

306 5 / 30 Fiber volume fraction
Con control denoting equivalent water addition as the respective composites
308 (-) non-sonicated samples
(+) sonicated samples

310

Figure 3: Compressive strength of the different samples. Notable is the consistently higher fracture
312 strength of the sonicated composites when compared to their non-sonicated counterparts or the pristine cements. Pristine samples are indicated by an x; the non-sonicated composites
314 by empty circles; and the sonicated composites by filled squares.

Con control denoting equivalent water addition as the respective composites
316 (-) non-sonicated samples
(+) sonicated samples

318

320 Figure 4: SEM micrographs of PLLA fiber reinforced cements with a) 5% v/v NF, c) 5% v/v MF, e) 30% v/v NF g) 30% v/v MF content, visible as single fibers exiting the cement at the
322 fracture area (white arrows as highlighted examples) and i) no fiber content. The respective

negative controls b), d), f), h) containing non-sonicated cut electrospun mats which are visible as fiber bundles existing the fracture area (red white ovals as highlighted examples).

Figure 5: Fracture area micrograph of composite with 5%v/v nanofibers a) and its corresponding Voronoi diagram (b).

Figure 6: Average Number of fibers per image on the fracture area of the sonicated composites. Notable is the similar high number in the nano fiber composites.

Table 1

	5% NF	5% MF	30% NF	30% MF
Average number of fibres per image $\bar{x}(f)$	180	25	190	55
Standard deviation +/- $\sigma(f)$	60	28	54	30
Coefficient of variation $\gamma(f)$	0.3	1.1	0.3	0.6
Voronoi surface area (um^2) $\bar{x}(v) \pm \sigma(v)$	16 ± 6	440 ± 740	14 ± 5	66 ± 36
Area homogeneity coefficient $\gamma(v) \pm \sigma(\gamma(v))$	1.0 ± 0.3	0.7 ± 0.4	0.8 ± 0.1	0.7 ± 0.2

Table 1: Average number of fibers as determined manually from the SEM micrographs. Voronoi surface areas as measured by software and calculated values as derived from section 2.6.

Figure 1:

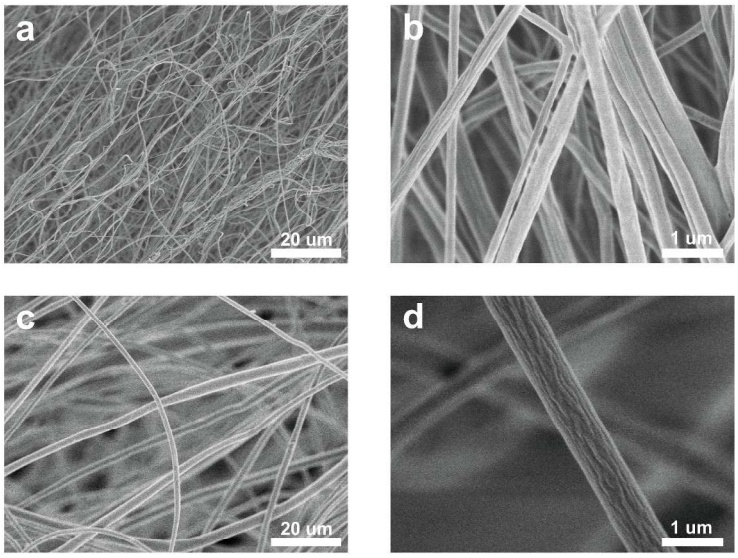

Figure 1:

SEM micrographs of pristine PLA NF (a, b) and MF (c, d) as spun on a rotating collector imaged at low (a, c) and high (b, d) magnification. Visible is the smooth structure of the NF b), and the wrinkled structure of the MF d).

279x361mm (300 x 300 DPI)

Figure 2:

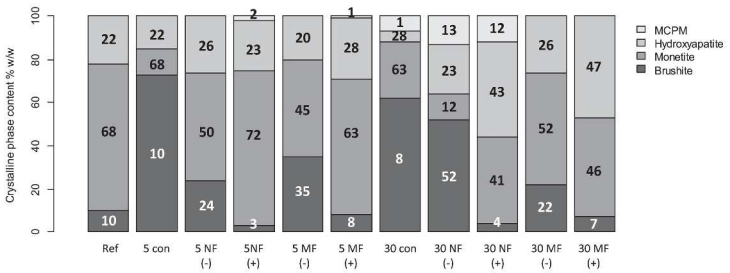

Figure 2:

XRD analysis of the relative (% mass) crystalline content of the sonicated composites. Brushite and monetite are the products, while MCPM and Hydroxyapatite are the starting materials. There is a trend of decrease in reactivity with increased fiber dispersion and fiber content. The numbers in the bars refer to respective mass fraction.

5 / 30 Fiber volume fraction
Con control denoting equivalent water addition as the respective composites
(-) non-sonicated samples
(+) sonicated samples

279x361mm (300 x 300 DPI)

Figure 3:

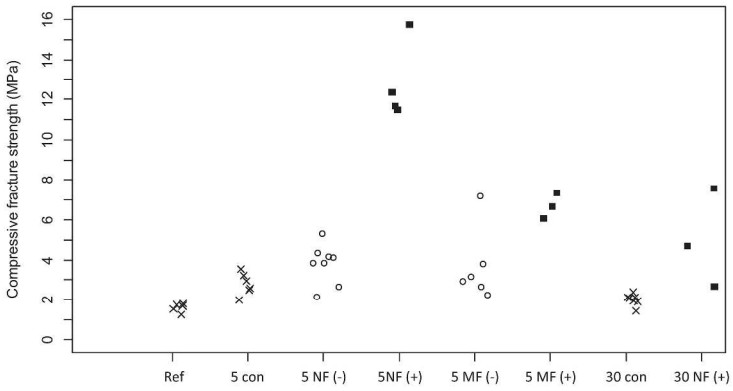

Figure 3:

Compressive strength of the different samples. Notable is the consistently higher fracture strength of the sonicated composites when compared to their non-sonicated counterparts or the pristine cements. Pristine samples are indicated by an x; the non-sonicated composites by empty circles; and the sonicated composites by filled squares.

Con control denoting equivalent water addition as the respective composites
(-) non-sonicated samples
(+) sonicated samples

279x361mm (300 x 300 DPI)

Figure 4:

Figure 4:

SEM micrographs of PLLA fiber reinforced cements with a) 5% v/v NF, c) 5% v/v MF, e) 30% v/v NF g) 30% v/v MF content, visible as single fibers exiting the cement at the fracture area (white arrows as highlighted examples) and i) no fiber content. The respective negative controls b), d), f), h) containing non-sonicated cut electrospun mats which are visible as fiber bundles existing the fracture area (red white ovals as highlighted examples).

(next page)

279x361mm (300 x 300 DPI)

Figure 4:

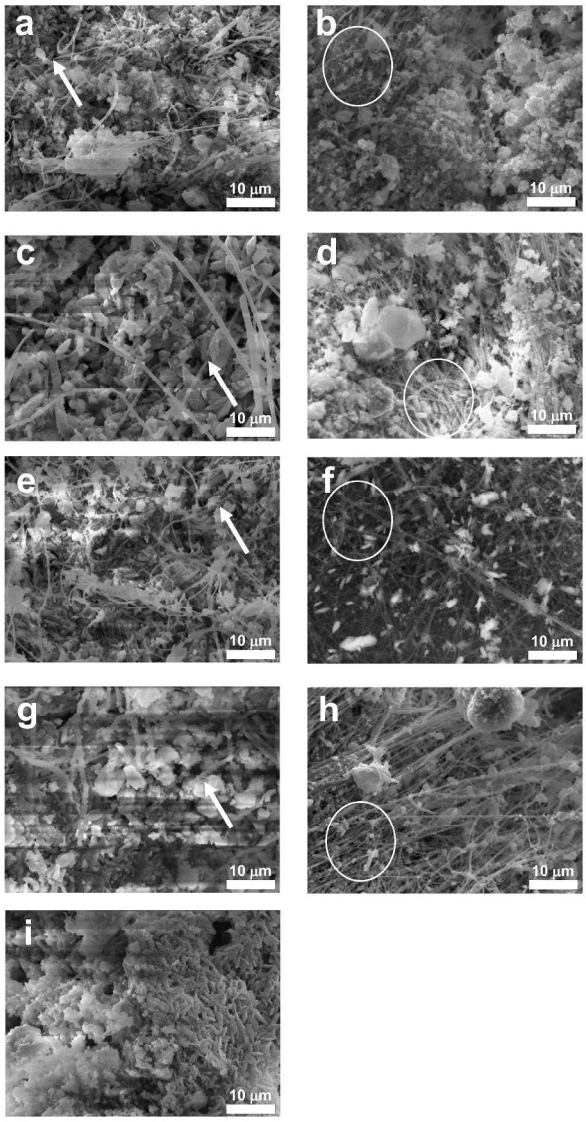

279x361mm (300 x 300 DPI)

Figure 5:

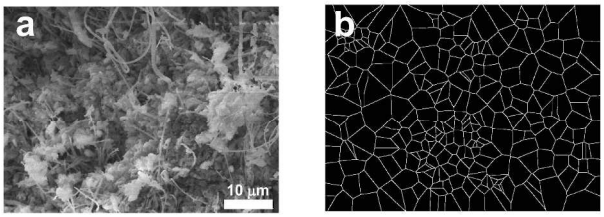

Figure 5:

Fracture area micrograph of composite with 5%v/v nanofibers a) and its corresponding Voronoi diagram (b).

279x361mm (300 x 300 DPI)

Figure 6:

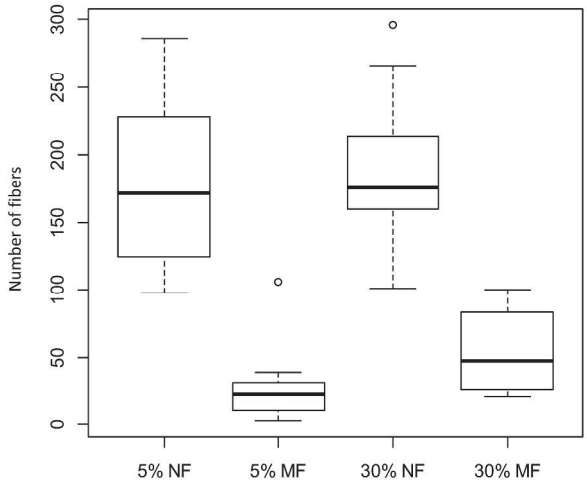

Figure 6:

Average Number of fibers per image on the fracture area of the sonicated composites. Notable is the similar high number in the nano fiber composites.

279x361mm (300 x 300 DPI)